ACS APPLIED MATERIALS & INTERFACES

Research Article

www.acsami.org

# Two-Phase Microfluidic Droplet Flows of Ionic Liquids for the Synthesis of Gold and Silver Nanoparticles

Laura L. Lazarus,[†,‡] Carson T. Riche,[†,§] Brandon C. Marin,[§] Malancha Gupta,[§] Noah Malmstadt,[*,§] and Richard L. Brutchey[*,‡]

[‡]Department of Chemistry, University of Southern California, Los Angeles, California 90089, United States

[§]Mork Family Department of Chemical Engineering and Materials Science, University of Southern California, Los Angeles, California 90089, United States

Supporting Information

**ABSTRACT:** Droplet-based microfluidic platforms have the potential to provide superior control over mixing as compared to traditional batch reactions. Ionic liquids have advantageous properties for metal nanoparticle synthesis as a result of their low interfacial tension and complexing ability; however, droplet formation of ionic liquids within microfluidic channels in a two-phase system has not yet been attained because of their complex interfacial properties and high viscosities. Here, breakup of an imidazolium-based ionic liquid into droplets in a simple two-phase system has for the first time been achieved and characterized by using a microchannel modified with a thin film fluoropolymer. This microfluidic/ionic liquid droplet system was used to produce small, spherical gold (4.28 ± 0.84 nm) and silver (3.73 ± 0.77 nm) nanoparticles.

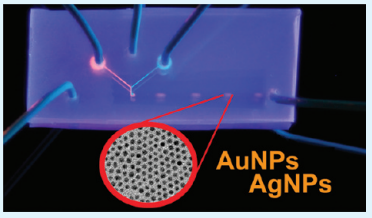


**KEYWORDS:** *gold, silver, nanoparticles, ionic liquids, microfluidics, vapor-phase polymerization*

Reactor miniaturization via microfluidic technology has enabled the continuous flow synthesis of a large number of molecules and nanomaterials.[1] Microfluidic reactors offer several advantages over traditional batch scale syntheses; namely, improved heat and mass transport in high surface area-to-volume microchannels, continuous throughput, superior reaction control, and minimal solvent waste and byproduct generation.[1,2] These features make microfluidic reactors uniquely suitable for producing tailor-made nanomaterials in high throughput with high fidelity.[3−5] Various continuous-flow configurations have been reported for the fabrication of metal nanoparticles including cobalt,[6] copper,[7] platinum and palladium,[8] gold and silver,[9] and core−shell particles.[10]

We previously demonstrated that gold nanoparticles could be synthesized in a microfluidic reactor by the flow-focused mixing of $HAuCl_4$ and $NaBH_4$ in the ionic liquid 1-butyl-3-methylimidazolium tetrafluoroborate (BMIM-$BF_4$).[11] Ionic liquids, such as those based on dialkylimidazolium cations (e.g., $BMIM^+$), have shown promise as dual-function solvents and stabilizing ligands for metal nanoparticles.[12,13] They are nonflammable, possess negligible vapor pressures, are chemically stable, and have low interfacial tensions that can result in high nucleation rates, all of which make them attractive solvents for nanoparticle synthesis.[14,15] Ionic liquids also have the ability to stabilize metal nanoparticles as a result of their high ionic charge and high dielectric constant.[16,17] Moreover, ionic liquids are fully compatible with poly(dimethylsiloxane) (PDMS)-based microfluidic devices, unlike many traditional organic solvents.[18]

Water-soluble acidic byproducts produced during synthesis can be a challenge to extract from water-miscible ionic liquids such as BMIM-$BF_4$, however. Some evidence also suggests $BF_4^-$ is prone to hydrolysis in the presence of water.[19] For the current study we chose 1-butyl-3-methylimidazolium bis-(trifluoromethylsulfonyl)imide (BMIM-$Tf_2N$) for the greater stability of the bistriflimide anion compared to tetrafluoroborate and for its hydrophobicity, making it easier to obtain in purer form. Substituting 1-butyl-3-methylimidazolium borohydride (BMIM-$BH_4$) for $NaBH_4$ also provides much improved reducing agent solubility in the ionic liquid without the possibility of forming sodium-containing byproducts.

Our previous work was based on reactions in narrow flow-focused laminar streams of reactants.[11] Although more controlled than mixing in a macroscale batch reactor, flow-focused laminar mixing within microchannels is diffusion-limited, and concentration gradients can lead to polydispersity in nanoparticle syntheses.[20−22] One solution to this problem is the use of droplet flows. Droplet flow microfluidic reactors allow for the generation of discrete droplets that are separated from one another by an inert, immiscible carrier phase. In this configuration, mixing within the droplet is rapid and can be precisely controlled, unlike in conventional macroscale batch reactors where mixing is almost always turbulent and not well-defined.[23,24] Droplet flows can eliminate concentration dispersion and maintain a constant ratio of reagents in all droplets. Convective mixing within these droplets has been shown to decrease the mixing time by 2 orders of magnitude as

Received: March 12, 2012
Accepted: April 23, 2012
Published: April 23, 2012

   dx.doi.org/10.1021/am3004413 | ACS Appl. Mater. Interfaces 2012, 4, 3077−3083

compared to diffusive mixing between coflowing laminar streams.[25] Despite these favorable conditions, very few droplet-based syntheses of metal nanoparticles have been reported to date and until now, small (i.e., <5 nm in diameter), monodisperse metal nanoparticles have not yet been achieved in droplet microreactors.[22,26,27]

Herein, we report the first microfluidic device designed for ionic liquid droplets in a two-phase flow. Droplet flows of ionic liquids are a new area of study in the microfluidics literature, and they represent an exceptional case of droplet flow behavior due to the complex interfacial properties and unusually high viscosity of the dispersed ionic liquid phase. Previously, breakup of an ionic liquid phase was achieved using a three-phase system in which an aqueous droplet supported an ionic liquid droplet.[28,29] An aqueous and ionic liquid stream were injected side by side and segmented to create compound droplets that appear to prevent the ionic liquid from contacting the channel walls. Herein, we report a microfluidic platform involving a simplified two-phase droplet flow for the continuous synthesis of high quality gold and silver nanoparticles (AuNPs and AgNPs, respectively), which involves fast, convective mixing between the metal salts and ionic liquid reducing agent in discrete droplets.

## RESULTS AND DISCUSSION

**Ionic Liquid Droplet Formation and Characterization.** Two-phase droplet flows offer ideal platforms for performing controlled synthesis of nanomaterials. The rate of mixing and type of mixing in discrete droplets separated by an immiscible carrier phase can be systematically tuned through varying the flow rates of the different phases. Breakup of an aqueous phase in a continuous oil phase has been well characterized; however, studies on the breakup of highly viscous dispersed phases in microfluidic channels are limited.[30−32] Here, stable droplet formation of the viscous BMIM-$Tf_2N$ ionic liquid within a continuous fluorocarbon oil phase, poly(chlorotrifluoroethylene) (PCTFE), was achieved by modifying the interior surfaces of preassembled PDMS devices with a fluoropolymer coating via a previously reported initiated chemical vapor deposition (iCVD) method.[33] Briefly, the poly(1*H*,1*H*,2*H*,2*H*-perfluorodecyl acrylate-co-ethylene glycol diacrylate) coating is deposited in a vapor phase polymerization process where monomer molecules and initiator radicals polymerize via a free-radical chain mechanism on the interior surfaces of the preassembled channels. Vapor phase polymerization improves upon previous methods for modifying preassembled channels by allowing for the modification of multiple devices simultaneously without the possibility of clogging channels, as can occur in liquid-phase processing. Additionally, the polymer film creates a barrier that completely masks the underlying PDMS and prevents hydrophobic recovery due to the low glass transition temperature of PDMS.[34] Coated devices performed with no signs of degradation or delamination for at least 24 h.

The fluoropolymer film allows the PCTFE carrier oil to preferentially wet the channel walls and provide a thin lubricating layer that prevents the ionic liquid droplets from directly contacting the channel walls. On native PDMS, BMIM-$Tf_2N$ has a static contact angle of 75°, which is well below the experimentally determined limit for droplet formation. Ionic liquid droplets do not form at any of the tested flow conditions in bare PDMS channels. After coating the PDMS with the fluoropolymer film, the contact angle increases to 110° as a result of the decreased surface energy of the fluoropolymer film compared to native PDMS. As a result of the complex interfacial properties of ionic liquids, the surface energy is difficult to predict a priori and varies significantly for different ionic liquids interacting with PDMS.

The droplet flow of two immiscible fluid phases in a multiple inlet T-junction device (Figure 1) was characterized to determine the optimal operating conditions for synthesizing monodisperse nanoparticles. Ionic liquid solutions of the metal salt precursor and the reductant were injected via inlets 2 and 4, respectively. To prevent diffuse mixing between reagent streams prior to droplet formation, we injected a pure BMIM-$Tf_2N$ stream between the two reagent streams via inlet 3. Convective mixing commenced once droplet formation occurred at the intersection of the dispersed phase and the immiscible oil. A phase diagram, constructed from images taken under different operating conditions, illustrates the dependence of the droplet formation process on the PCTFE oil flow rate and the ratio of the reagent flow rate (dispersed phase) to the oil flow rate (continuous phase) (Figure 2A). All flows were allowed to stabilize and each outlined set of micrographs depicts the breakup process for a single droplet at the indicated conditions. In the dripping regime, droplet breakup occurs within a channel width of the injection point (outlined in green).[35] At higher carrier flow rates and higher flow rate ratios ($\geq$6 mL $h^{-1}$ and $\geq$1/5, respectively), droplets pinch off further downstream at the end of an extended strand, a phenomenon known as jetting.

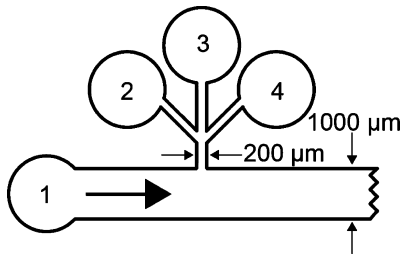


**Figure 1.** Schematic representation of the multiple inlet T-junction microfluidic device used to synthesize Au and AgNPs. The carrier oil was injected via inlet 1 while the reagent streams were introduced via inlets 2 and 4. A pure BMIM-$Tf_2N$ stream was injected via inlet 3 to prevent diffusive mixing between reagent streams before droplet formation could occur. The intrachannel arrow indicates the direction of droplet flow.

A combination of convective and diffusive mixing occurs within each droplet. With jetting, or at even higher flow rates where droplets could not be formed, diffusive mixing dominates across the width of the channel, leading to an inhomogeneous concentration of reagents in a droplet. This prolongs the nucleation burst and produces more polydisperse nanoparticles.[36] It is preferable to operate in the dripping regime, where droplets form at the channel junction and droplet sizes are more controllable and uniform.[37] In this regime, convective mixing − induced by recirculating streamlines caused by the no-slip boundary conditions at the channel wall − results in fluid layering within the droplet. Layering effectively reduces the distance over which species are required to diffuse in order to mix. Decreasing the lengths over which diffusion occurs leads to more rapid homogenization of reagents in the droplet. The time scale for diffusive transport is inversely proportional to the diffusivity of the desired species and the time scale for

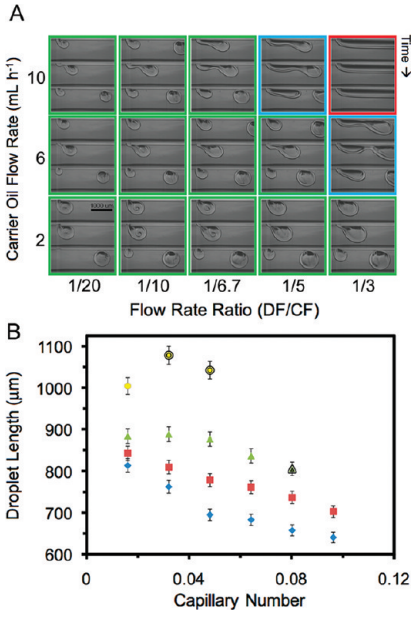


**Figure 2.** (A) Phase diagram indicating dependence of droplet formation on relationship between carrier oil flow rate and flow rate ratio of dispersed phase (DF) and continuous phase (CF) flow rates. Each panel shows three time points in the formation and break-off of a single droplet at the indicated conditions. Dripping regime conditions are outlined in green, jetting regime conditions in blue, and nondroplet-forming conditions in red. (B) Characterization of droplet size as a function of capillary number for certain flow rate ratios of 1/10 (diamonds), 1/6.7 (squares), 1/5 (triangles), and 1/3 (circles). Outlined shapes indicate the jetting regime droplets as highlighted in blue in A. The sizes are given as the lengths of droplets in the direction of flow, measured 1 cm from the injection point.

convective transport is inversely proportional to the velocity of the droplet.[38] Consequently, the dominant form of mixing can be estimated from the droplet velocity and the diffusivity of droplet species. The self-diffusion of BMIM-$Tf_2N$ is an estimate of the upper limit for diffusivity at $1 \times 10^{-7}$ $cm^2$ $s^{-1}$.[39] For this value and our channel geometry, the critical interlayering velocity (defined as the limit at which convective mixing begins to dominate) would be below the droplet velocity for any of the flow conditions tested.[38] Also, operating at the higher PCTFE flow rates would shift mixing further into the convection-dominated regime. A larger flow rate ratio increases throughput; therefore, we chose an oil flow rate of 10 mL $h^{-1}$ and reagent flow rates of 0.5 mL $h^{-1}$ (total dispersed phase flow rate = 1.5 mL $h^{-1}$). Additionally, conditions were chosen such that the emerging interface filled less than half the width of the main channel before breaking off into droplets. This avoids significant droplet/wall interaction as well as perturbations in the flow as shear stress drives droplet formation in this regime, not pressure accumulating upstream from the emerging droplet.

The size of each droplet was measured a third of the way down the channel for conditions shown to produce stable droplet formation (Figure 2B). Droplet lengths varied by <3% in all cases, indicating that the syringe pumps were operating properly and syringes were adequately sized. Trends in droplet size correlated well with those reported for aqueous streams where droplet length was shown to decrease with increasing capillary number and viscous force.[37] The dimensionless capillary number ($Ca$) is a ratio of viscous stress to interfacial tension where $\mu$ is the viscosity of the dispersed phase, $V$ is the linear velocity, and $\gamma$ is the interfacial tension.[40]

$$Ca = V\mu/\gamma$$

The viscosity of the dispersed phase reaction mixture (39.09 ± 0.65 mPa s for AuNP reagent droplets) was used to calculate $Ca$ since this allows for future comparison of viscous dispersed phases (i.e., various ionic liquids) with different viscosities using the same carrier fluid. Altering the precursor solutions for various syntheses will affect the dispersed phase viscosity. For example, the AgNP reagent droplets contain less 1-methylimidazole, resulting in a small shift to higher viscosity. Overall, the range of stable droplet formation is shifted to higher values of $Ca$ when compared with the breakup process for aqueous phases.[32] The jump in droplet size for a flow rate ratio of 1:3 can be attributed to a transition from the dripping to jetting regime, as indicated in the phase diagram. This transition occurs at $Ca$ ~0.02 for a flow rate ratio of 1/3 and at $Ca$ ~0.07 for a flow rate ratio of 1/5. For a given $Ca$, higher flow rate ratios resulted in larger droplets, as expected from the droplet growing faster at a higher dispersed phase flow rate.

**Au and Ag Nanoparticle Synthesis and Characterization.** Under optimal droplet flow conditions each of the 3-branched inlet streams (Figure 1, inlets 2–4) had flow rates of 0.5 mL $h^{-1}$, whereas the continuous phase (inlet 1) was injected at 10 mL $h^{-1}$. Au and AgNPs were synthesized on device by first preparing BMIM-$Tf_2N$ solutions of the metal salt ($HAuCl_4 \cdot xH_2O$ or $AgBF_4$), 1-methylimidazole, and BMIM-$BH_4$ with the appropriate concentrations (*vide infra*). The BMIM-$BH_4$ reducing agent rapidly forms a homogeneous solution in BMIM-$Tf_2N$, circumventing solubility issues associated with $NaBH_4$ solutions in ionic liquid solvents. The $HAuCl_4$ or $AgBF_4$ solutions in BMIM-$Tf_2N$ were thoroughly mixed with an equal volume of 1-methylimidazole solution in BMIM-$Tf_2N$ prior to injection on device via inlet 2 (Figure 1). The addition of 1-methylimidazole was necessary to achieve nonagglomerated nanoparticles with homogeneous morphologies. A common impurity in ionic liquids, 1-methylimidazole has been shown to bind to metal surfaces and can serve as an acid scavenger, preventing the build up of acidic byproducts that may destabilize nanoparticles and promote aggregation.[41,42] The BMIM-$BH_4$ solution was introduced via inlet 4 and a pure BMIM-$Tf_2N$ buffer stream was injected via inlet 3 to prevent diffusive mixing between reagents before droplet formation occurred. Synthesized AuNPs were washed thoroughly with ethanol to remove excess BMIM-$Tf_2N$ and BMIM-$BH_4$ and redispersed in hexanes with 1-dodecanethiol. AgNPs were phase transferred to hexanes with 1-dodecanethiol and trioctylamine and precipitated with ethanol several times to remove excess ionic liquid solvent and reducing agent. For comparison, batch reactions were performed by stirring the above solutions in the same reagent ratios with reaction times that matched the residence time on device.

The formation of Au and AgNPs was confirmed by the observance of characteristic localized surface plasmon resonances (LSPR) in their absorption spectra. Red colored suspensions of AuNPs synthesized on device exhibited relatively narrow LSPR bands centered at $\lambda$ = 519 nm (fwhm = 172 nm), typical of nonagglomerated, spherical AuNPs (Figure 3).[43] The AuNPs produced in an analogous batch reaction displayed a broadened and red-shifted LSPR band ($\lambda$ = 523 nm, fwhm = 197 nm), indicative of larger and more polydisperse nanoparticles.


dx.doi.org/10.1021/am3004413 | ACS Appl. Mater. Interfaces 2012, 4, 3077–3083

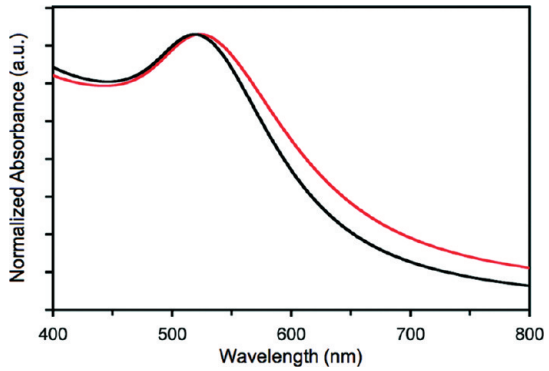


**Figure 3.** Normalized UV−vis spectra of AuNPs produced on device (black) and in a conventional batch reaction (red).

The size, morphology, and size distribution of resulting nanoparticles were characterized by transmission electron microscopy (TEM). TEM micrographs were processed in Matlab to analyze nanoparticle size and shape statistics. Nanoparticle diameters were calculated based on the projected area, in a manner consistent with NIST protocol.[44] Grayscale images were converted to binary images with discrete nanoparticles on a uniform background, using a consistent thresholding technique for an accurate comparison of separate samples.

The AuNPs synthesized on device under optimal droplet flow conditions were spherical and monodisperse with a mean diameter of 4.28 ± 0.84 nm ($n$ = 54 684), with average major and minor axis lengths of 4.78 and 4.13 nm, respectively (Figure 4A) (see the Supporting Information for analysis at additional conditions). The nanoparticles exhibited an ellipticity of 1.16, defined as the major axis length/minor axis length. The AuNPs produced in an analogous batch reaction were larger with a mean diameter of 5.52 ± 0.98 nm ($n$ = 57 732) and average major and minor axis lengths of 6.09 and 5.18 nm, respectively (Figure 4B). The AuNPs produced in the batch reaction possessed an ellipticity of 1.18. We statistically analyzed the populations of AuNPs synthesized on device and in batch. A Kolmogorov−Smirnov test[45] revealed the distributions of the diameters ($p_{device}$ = 0, $p_{batch}$ = 0) were non-normal for all groups. Therefore, a nonparametric Wilcoxon rank sum test[46] was used to demonstrate that the diameters of the AuNPs produced in batch were significantly larger than the diameters of the nanoparticles produced on device ($z$ = 196, $p$ = 0). The AuNPs synthesized in batch were 29% larger than those produced in the microfluidic device. In addition, the major and minor axes of the AuNPs produced on device were statistically smaller than their analogues synthesized in the batch reaction. Fast and efficient mixing within droplets promotes a short nucleation burst and a more homogeneous reaction environment, as compared with batch scale mixing with a magnetic stir bar where homogenization takes more than a minute.[47]

The same general procedure was used to synthesize small AgNPs. The AgNPs produced on device exhibited distinctive LSPR bands centered at $\lambda$ = 436 nm with a small shoulder centered at $\lambda$ = 346 nm (Figure 5C).[48] In the analogous batch reaction, the absorption spectra of the resulting AgNPs is dominated by the band centered at $\lambda$ = 343 nm, with a less intense, broadened, and slightly blue-shifted LSPR band ($\lambda$ = 431 nm) as compared to the AgNPs made on device (Figure

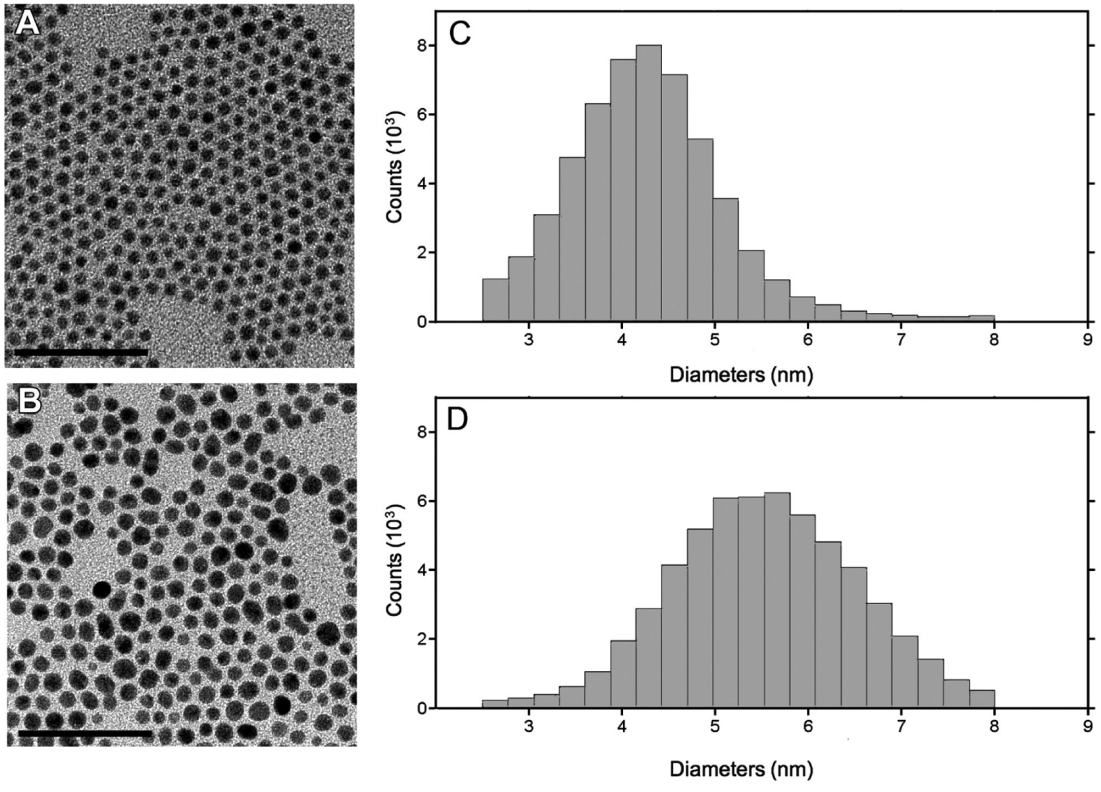


**Figure 4.** TEM micrographs of AuNPs produced (A) in a droplet-based microfluidic device and (B) in an analogous batch reaction. Scale bars are 50 nm. Histograms of AuNP diameters show that nanoparticles produced (C) on the device were smaller with a narrower size distribution compared to (D) those produced in batch.

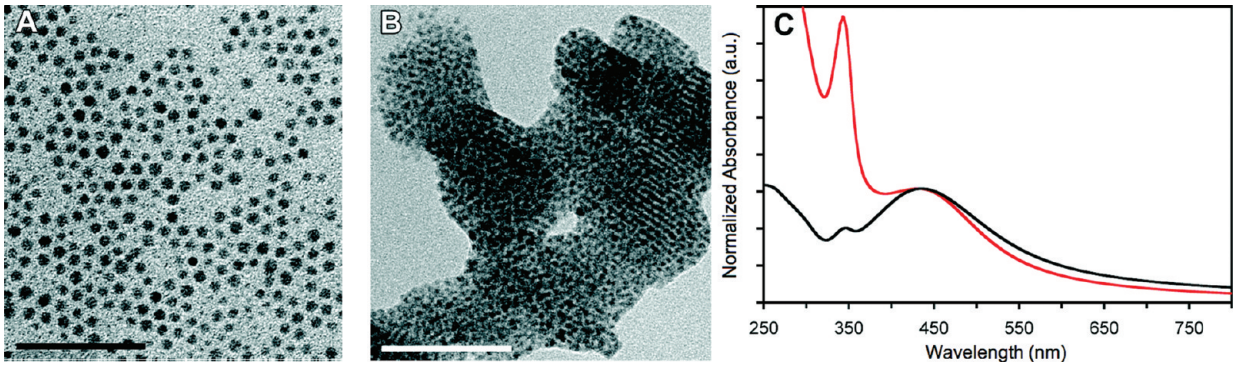


**Figure 5.** TEM micrographs of AgNPs produced (A) in a droplet-based microfluidic device and (B) in an analogous batch reaction. Scale bars are 50 nm. (C) UV−vis spectra of AgNPs produced on device (black) and in a batch reaction (red).

5C). It is worthwhile to note that for reactions on device and in batch, the absorbance band observed at ca. 350 nm increased in intensity with increasing 1-methylimidazole concentration (see the Supporting Information, Figure S1) and the reactions were perceived to slow, as qualitatively judged by color. The intensity of this peak was also observed to increase with decreasing residence time on device (see the Supporting Information, Figure S2). This band has previously been attributed to magic-sized silver clusters of different sizes.[49−52] It is likely that the absorbance band we observe *ca.* 350 nm is similarly due to silver clusters of less than 10 atoms that serve as intermediates to AgNPs, and that rapid mixing in the droplet flow accounts for the differences in the two products achieved via the microfluidic reaction versus the analogous batch reaction (with identical 1-methylimidazole concentrations).

The end-result AgNPs synthesized on device had a mean diameter of 3.73 ± 0.77 nm ($n$ = 30 249) with major and minor axis lengths of 4.65 and 3.68 nm, respectively (Figure 5A). Striking differences were observed for AgNPs synthesized in batch. Whereas well-defined spherical AgNPs were produced on device, the same conditions in batch produced large coral-like assemblies of very small AgNPs (<2 nm in diameter, Figure 5B). The presence of Moiré fringes suggests short-range order characteristic of nanoparticle superlattices.[53−56]

As in the synthesis of AuNPs, 1-methylimidazole provided an additional stabilization effect that resulted in more uniform nanoparticle morphologies that were largely nonagglomerated. However, unlike AuNP synthesis, much lower concentrations of 1-methylimidazole were required to achieve well-defined spherical AgNPs. It is likely that the acidic byproducts formed in the reaction of $HAuCl_4{\cdot}xH_2O$ necessitate higher concentrations of an acid-scavenger such as 1-methylimidazole for stabilization of AuNPs compared to AgNPs.

## CONCLUSIONS

Small, monodisperse Au and AgNPs were fabricated in an ionic liquid solvent using a simple droplet-based microfluidic device. Various flow conditions were analyzed to determine optimal flow rates for producing droplets whose contents were quickly homogenized by convection-dominated mixing. Well-dispersed spherical nanoparticles were obtained that were smaller and more monodisperse than those produced in analogous batch reactions as a result of the rapid mixing and the homogeneous reaction environment afforded by the discrete droplets within an immiscible carrier phase. Very few droplet-based microfluidic syntheses of metal nanoparticles have been reported[22,26,27] and Au and AgNPs synthesized in microfluidic reactors under various aqueous or organic flow regimes have resulted in nanoparticles that were larger and more polydisperse or were produced under harsher reaction conditions (e.g., elevated temperatures).[57−60] Our work demonstrates that the combination of fast and controlled microfluidic mixing with ionic liquid solvents allows for the synthesis of high-quality, small, monodisperse Au and AgNPs under very benign conditions. This opens the possibility of such platforms being used for nanomanufacturing metal nanoparticles using inexpensive, rapid, and reproducible methods that have minimal impact on the environment.

## MATERIALS AND METHODS

**Chemicals.** Hydrogen tetrachloroaurate(III) hydrate ($HAuCl_4{\cdot}xH_2O$, 99.999%), silver(I) tetrafluoroborate ($AgBF_4$, 98%), sodium borohydride ($NaBH_4$, 99%), trioctylamine (98%), and 1-butyl-3-methylimidazolium bromide (BMIM-Br, ≥97%) were purchased from Sigma-Aldrich. 1-butyl-3-methylimidazolium bis-(trifluoromethylsulfonyl)imide (BMIM-$Tf_2N$, 99%) was purchased from IOLITEC Inc. (Tuscaloosa, AL). The as-purchased BMIM-$Tf_2N$ was analyzed and found to contain <9 ppm chloride and <161 ppm water by suppressed ion chromatography and Karl Fischer titration methods, respectively (Galbraith Laboratories, Inc.; Knoxville, TN). 1-Methylimidazole (99%) and 1-dodecanethiol (98%) were purchased from Alfa-Aesar. Inert poly(chlorotrifluoroethylene) oil (Halocarbon 6.3) was purchased from Halocarbon (River Edge, NJ). All chemicals were used as received without further purification.

**Synthesis of 1-Butyl-3-methylimidazolium borohydride (BMIM-$BH_4$).** BMIM-$BH_4$ was synthesized following a literature procedure.[61] Briefly, BMIM-Br (5.14 g, 23.5 mmol) and $NaBH_4$ (1.07 g, 28.1 mmol) were stirred in dry acetonitrile for 24 h at 25 °C under an atmosphere of nitrogen. The colorless solution was separated from the NaBr byproduct via cannula filtration and then dried in vacuo to yield the BMIM-$BH_4$ product (3.53 g, 97.4% isolated yield) as a low melting solid. The product appears to be stable for long periods of time when stored under nitrogen. $^1$H NMR (500 MHz, DMSO-$d_6$, $\delta$): 9.15 (s, 1H), 7.78 (s, 1H), 7.71 (s, 1H), 4.17 (t, 2H), 3.85 (s, 3H), 1.80−1.74 (m, 2H), 1.30−1.22 (m, 2H), 0.90 (t, 3H), −0.06−0.55 ($BH_4$). $^{13}$C NMR (125 MHz, DMSO-$d_6$, $\delta$): 136.4, 123.5, 122.2, 48.4, 35.6, 31.2, 18.7, 13.2.

**Microfluidic Device Fabrication.** Standard photolithography techniques were used to create a SU-8 50 photoresist (MicroChem) mold on a silicon wafer from an emulsion transparency mask (CAD/Art Services, Inc.). The completed mold was exposed to trichloro-(1*H*,1*H*,2*H*,2*H*-perfluorooctyl)silane (Sigma-Aldrich) in a desiccator for 20 min. A 2-mm thick layer of Sylgard 182 (10:1 base/cross-linker ratio, Dow Corning) was cast onto the mold and cured in an oven at 65 °C for 4 h. The devices were assembled by oxidizing both the patterned surface and a 2-mm thick slab of blank PDMS with a corona generator (BD20-AC, Electro-Technic Products, Inc.), pressing the layers together, and curing the device in an oven at 65 °C for 4 h. A

typical device measured 2 × 4 cm overall and the channel depth, main channel width, and channel width at the branched inlets were 450, 1000, and 200 μm, respectively.

**Vapor Phase Polymerization onto Microfluidic Devices.** The preassembled microfluidic devices were modified via initiated chemical vapor deposition (iCVD) in a custom-designed reaction chamber (GVD Corporation). Monomer and initiator molecules were continuously flowed into the chamber where a heated wire array thermally decomposed initiator molecules into free radicals. These radicals and the monomer molecules diffused into the channels via the channel inlets, adsorbed to the cooled PDMS surfaces, and polymerized via a free radical chain mechanism. In order to ensure that the coating penetrated the entire channel, the reactor pressure was kept at 50 mTorr, the stage temperature was kept at 30 °C, and the wire filament temperature was kept at 200 °C. The di-*tert*-butyl peroxide initiator (Sigma-Aldrich, 98%), 1*H*,1*H*,2*H*,2*H*-perfluorodecyl acrylate monomer (SynQuest, 97%), and ethylene glycol diacrylate cross-linker (Sigma-Aldrich, 90%) were all used as received. The flow rates of the three were 2.6, 0.2, and 0.7 standard cubic centimeters per minute, respectively.

**Microfluidic Synthesis of Au Nanoparticles.** Solutions of $HAuCl_4$ (10 mM), 1-methylimidazole (5 M), and BMIM-$BH_4$ (0.1 M) were prepared in BMIM-$Tf_2N$ with stirring at 25 °C. Equal volumes of $HAuCl_4$ and 1-methylimidazole solutions were thoroughly mixed before being introduced on device via syringe pump. Syringes and outlet tubing interfaced with the microfluidic device via PEEK tubing (I.D. = 0.762 mm) and exited the device via silicon tubing (I.D. = 1.02 mm). Reagent solutions of $HAuCl_4$/1-methylimidazole and BMIM-$BH_4$ were injected through inlets 2 and 4, respectively. A pure BMIM-$Tf_2N$ buffer stream was injected between the two reagent streams via inlet 3. All dispersed phase reagents had a flow rate of 0.5 mL $h^{-1}$. The immiscible carrier oil, poly(chlorotrifluoroethylene) (PCTFE) was injected into the main channel with a flow rate of 10 mL $h^{-1}$ via inlet 1. The samples exited the microfluidic device and were collected for 30 min in an empty collection tube (residence time = 60 s) where they separated into two distinct phases and the oil phase was removed prior to workup. The AuNPs were precipitated by centrifugation after the addition of ethanol (4 mL). The colorless supernatant was replaced with fresh ethanol and the mixture was sonicated for 2 min using a probe sonicator fitted with a microtip at 50% duty cycle (Sonifier S-450A analog ultrasonic processor, Branson). The AuNPs were again isolated by centrifugation and finally redispersed in hexanes and 1-dodecanethiol (10−20 μL $mL^{-1}$ hexanes) with probe sonication for 1 min.

**Microfluidic Synthesis of Ag Nanoparticles.** Solutions of $AgBF_4$ (40 mM), 1-methylimidazole (1.2 M), and BMIM-$BH_4$ (200 mM) were prepared in BMIM-$Tf_2N$ with stirring at 25 °C. Equal volumes of $AgBF_4$ and 1-methylimidazole solutions were thoroughly mixed before being introduced on device via syringe pump. Reagent solutions of $AgBF_4$/1-methylimidazole and BMIM-$BH_4$ were injected through inlets 2 and 4, respectively. Solutions containing the $AgBF_4$ were protected from light until before the reaction. A pure BMIM-$Tf_2N$ buffer stream was injected between the two reagent streams via inlet 3. All dispersed phase inlets had a flow rate of 0.5 mL $h^{-1}$. The immiscible carrier oil was injected into the main channel with a flow rate of 10 mL $h^{-1}$ via inlet 1. The AgNPs were isolated by phase transfer whereby the AgNP dispersion in BMIM-$Tf_2N$ was collected into an organic phase containing hexanes (2 mL), ethanol (2 mL), 1-dodecanethiol (50 μL), and trioctylamine (25 μL). The samples were collected for 30 min (residence time =2 min 45 s) and the colored organic layer containing AgNPs was transferred to a new centrifuge tube. The AgNPs were precipitated by centrifugation after the addition of methanol (3 mL). The colorless supernatant was replaced with ethanol and the mixture was sonicated for 2 min using a probe sonicator fitted with a microtip at 50% duty cycle. The AgNPs were again isolated by centrifugation and finally redispersed in hexanes (1−2 mL) with probe sonication for 1 min.

**Batch Synthesis of Au and Ag Nanoparticles.** Solutions of $HAuCl_4$ (10 mM), 1-methylimidazole (5 M), and BMIM-$BH_4$ (0.1 M) were prepared in BMIM-$Tf_2N$ with stirring at 25 °C. Solutions of $HAuCl_4$ (0.25 mL) and 1-methylimidazole (0.25 mL) were thoroughly mixed. Thereafter, 0.5 mL of the BMIM-$BH_4$ solution was rapidly injected resulting in an immediate color change. After stirring for 1 min the AuNPs were precipitated by centrifugation with the addition of ethanol (4 mL). The colorless supernatant was replaced with fresh ethanol and the mixture was sonicated for 2 min using a probe sonicator fitted with a microtip at 50% duty cycle. The AuNPs were again isolated by centrifugation and finally redispersed in hexanes and 1-dodecanethiol (10−20 μL $mL^{-1}$ hexanes) with probe sonication for 1 min.

For the synthesis of AgNPs, solutions of $AgBF_4$ (40 mM), 1-methylimidazole (1.2 M) and BMIM-$BH_4$ (200 mM) were prepared in BMIM-$Tf_2N$ with stirring at 25 °C. Solutions of $AgBF_4$ (0.25 mL) and 1-methylimidazole (0.25 mL) in BMIM-$Tf_2N$ were thoroughly mixed in the absence of light. Thereafter, a solution of BMIM-$BH_4$ in BMIM-$Tf_2N$ (0.5 mL) was rapidly injected resulting in a color change after *ca.* 10 s. The AgNPs were isolated by phase transfer whereby the AgNP dispersion in BMIM-$Tf_2N$ was collected into an organic phase containing hexanes (2 mL), ethanol (2 mL), 1-dodecanethiol (50 μL), and trioctylamine (25 μL). The colored organic phase containing AgNPs was separated and the AgNPs precipitated by centrifugation with the addition of methanol (3 mL). The colorless supernatant was replaced with ethanol and the mixture was sonicated for 2 min using a probe sonicator fitted with a microtip at 50% duty cycle. The AgNPs were again isolated by centrifugation and finally redispersed in hexanes (1−2 mL) with probe sonication for 1 min.

**Characterization.** TEM was performed on a JEOL JEM-2100 electron microscope at an operating voltage of 200 kV, equipped with a Gatan Orius CCD camera. UV−vis absorption spectra were collected on a Shimadzu UV-1800 spectrophotometer in dual beam mode using quartz cuvettes with 1-cm path lengths from nanoparticle dispersions in hexanes. NMR spectra were collected on a Varian VNMRS-500 2-Channel NMR spectrometer at 25 °C. Viscosity was measured using a Cannon-Ubbelohde viscometer at room temperature. The liquid mixture was composed of the reagent solutions for AuNP synthesis with the $HAuCl_4$ solution replaced by pure BMIM-$Tf_2N$ to prevent gold nanoparticle formation.

## ■ ASSOCIATED CONTENT

### Ⓢ Supporting Information

Additional UV−vis spectra and additional size distributions of AuNPs at other flow conditions. This material is available free of charge via the Internet at http://pubs.acs.org.

## ■ AUTHOR INFORMATION

### Corresponding Author

*E-mail: malmstad@usc.edu (N.M.); brutchey@usc.edu (R.L.B.).

### Author Contributions

†These authors contributed equally to this work.

### Notes

The authors declare no competing financial interest.

## ■ ACKNOWLEDGMENTS

This material is based on work supported by the National Science Foundation under CMMI-0926969. R. L. B. acknowledges the Research Corporation for Science Advancement for a Cottrell Scholar Award. C. T. R. is supported by a fellowship from the Chevron Corporation (USC−CVX UPP).

## ■ REFERENCES

(1) Song, H.; Chen, D. L.; Ismagilov, R. F. *Angew. Chem., Int. Ed.* **2006**, *45*, 7336−7356.

(2) DeMello, A. J. *Nature* **2006**, *442*, 394−402.

(3) Jahn, A.; Reiner, J. E.; Vreeland, W. N.; DeVoe, D. L.; Locascio, L. E.; Gaitan, M. *J. Nanopart. Res.* **2008**, *10*, 925−934.

(4) Song, Y.; Hormes, J.; Kumar, C. S. S. R. *Small* **2008**, *4*, 698−711.
(5) Zhao, C.-X.; He, L.; Qiao, S. Z.; Middelberg, A. P. J. *Chem. Eng. Sci.* **2011**, *66*, 1463−1479.
(6) Song, Y.; Modrow, H.; Henry, L. L.; Saw, C. K.; Doomes, E. E.; Palshin, V.; Hormes, J.; Kumar, C. S. S. R. *Chem. Mater.* **2006**, *18*, 2817−2827.
(7) Song, Y.; Doomes, E. E.; Prindle, J.; Tittsworth, R.; Hormes, J.; Kumar, C. S. S. R. *J. Phys. Chem. B* **2005**, *109*, 9330−9338.
(8) Scheeren, C. W.; Machado, G.; Teixeira, S. R.; Morais, J.; Domingos, J. B.; Dupont, J. *J. Phys. Chem. B* **2006**, *110*, 13011−13020.
(9) Wagner, J.; Tshikhudo, T. R.; Köhler, J. M. *Chem. Eng. J.* **2008**, *135S*, S104−S109.
(10) Knauer, A.; Thete, A.; Li, S.; Romanus, H.; Csáki, A.; Fritzsche, W.; Köhler, J. M. *Chem. Eng. J.* **2011**, *166*, 1164−1169.
(11) Lazarus, L. L.; Yang, A. S.-J.; Chu, S.; Brutchey, R. L.; Malmstadt, N. *Lab Chip* **2010**, *10*, 3377−3379.
(12) Neouze, M.-A. *J. Mater. Chem.* **2010**, *20*, 9593−9607.
(13) Marquardt, D.; Xie, Z.; Taubert, A.; Thomann, R.; Janiak, C. *Dalton Trans.* **2011**, *40*, 8290−8293.
(14) Dupont, J.; Scholten, J. D. *Chem. Soc. Rev.* **2010**, *39*, 1780−1804.
(15) Ma, Z.; Yu, J.; Dai, S. *Adv. Mater.* **2010**, *22*, 261−285.
(16) Hardacre, C.; Holbrey, J. D.; McMath, S. E. J.; Bowron, D. T.; Soper, A. K. *J. Chem. Phys.* **2003**, *118*, 273−278.
(17) Dupont, J.; Suarez, P. A. Z. *Phys. Chem. Chem. Phys.* **2006**, *8*, 2441−2452.
(18) Lee, J. N.; Park, C.; Whitesides, G. M. *Anal. Chem.* **2003**, *75*, 6544−6554.
(19) Freire, M. G.; Neves, C. M. S. S.; Marrucho, I. M.; Coutinho, J. A. P.; Fernandes, A. M. *J. Phys. Chem. A* **2010**, *114*, 3744−3749.
(20) Hung, L.-H.; Choi, K. M.; Tseng, W.-Y.; Tan, Y.-C.; Shea, K. J.; Lee, A. P. *Lab Chip* **2006**, *6*, 174−178.
(21) Li, S.; Xu, J.; Wang, Y.; Luo, G. *Langmuir* **2008**, *24*, 4194−4199.
(22) Duraiswamy, S.; Khan, S. A. *Small* **2009**, *5*, 2828−2834.
(23) Frenz, L.; El Harrak, A.; Pauly, M.; Bégin-Colin, S.; Griffiths, A. D.; Baret, J.-C. *Angew. Chem., Int. Ed.* **2008**, *47*, 6817−6820.
(24) Teh, S.-Y.; Lin, R.; Hung, L.-H.; Lee, A. P. *Lab Chip* **2008**, *8*, 198−220.
(25) Tice, J. D.; Song, H.; Lyon, A. D.; Ismagilov, R. F. *Langmuir* **2003**, *19*, 9127−9133.
(26) Sotowa, K.-I.; Irie, K.; Fukumori, T.; Kusakabe, K.; Sugiyama, S. *Chem. Eng. Technol.* **2007**, *30*, 383−388.
(27) Nightingale, A. M.; Krishnadasan, S. H.; Berhanu, D.; Niu, X.; Drury, C.; McIntyre, R.; Valsami-Jones, E.; deMello, J. C. *Lab Chip* **2011**, *11*, 1221−1227.
(28) Barikbin, Z.; Rahman, Md. T.; Parthiban, P.; Rane, A. S.; Jain, V.; Duraiswamy, S.; Lee, S. H.; Khan, S. A. *Lab Chip* **2010**, *10*, 2458−2463.
(29) Feng, X.; Yi, Y.; Yu, X.; Pang, D.-W.; Zhang, Z.-L. *Lab Chip* **2010**, *10*, 313−319.
(30) Thorsen, T.; Roberts, R. W.; Arnold, F. H.; Quake, S. R. *Phys. Rev. Lett.* **2001**, *86*, 4163−4166.
(31) Garstecki, P.; Fuerstman, M. J.; Stone, H. A.; Whitesides, G. M. *Lab Chip* **2006**, *6*, 437−446.
(32) Tice, J. D.; Lyon, A. D.; Ismagilov, R. F. *Anal. Chim. Acta* **2004**, *507*, 73−77.
(33) Riche, C. T.; Marin, B. C.; Malmstadt, N.; Gupta, M. *Lab Chip* **2011**, *11*, 3049−3052.
(34) Zhou, J.; Ellis, A. V.; Voelcker, N. H. *Electrophoresis* **2010**, *31*, 2−16.
(35) Baroud, C. N.; Gallaire, F.; Dangla, R. *Lab Chip* **2010**, *10*, 2032−2045.
(36) Song, H.; Tice, J. D.; Ismagilov, R. F. *Angew. Chem., Int. Ed.* **2003**, *42*, 768−772.
(37) Christopher, G. F.; Noharuddin, N. N.; Taylor, J. A.; Anna, S. L. *Phys. Rev. E* 2008, *78* Article No. 036317.
(38) Handique, K.; Burns, M. A. *J. Micromech. Microeng.* **2001**, *11*, 548−554.
(39) Rollet, A.-L.; Porion, P.; Vaultier, M.; Billard, I.; Deschamps, M.; Bessada, C.; Jouvensal, L. *J. Phys. Chem. B* **2007**, *111*, 11888−11891.
(40) Chan, E. M.; Alivisatos, A. P.; Mathies, R. A. *J. Am. Chem. Soc.* **2005**, *127*, 13854−13861.
(41) Redel, E.; Thomann, R.; Janiak, C. *Inorg. Chem.* **2008**, *47*, 14−16.
(42) Dash, P.; Scott, R. W. J. *Chem. Commun.* **2009**, 812−814.
(43) Ghosh, S. K.; Pal, T. *Chem. Rev.* **2007**, *107*, 4797−4862.
(44) Bonevich, S. K.; Haller, W. K. In *NIST − NCL Joint Assay Protocol, PCC-7: Measuring the Size of Nanoparticles Using Transmission Electron Microscopy*; National Institute of Standards and Technology: Gaithersburg, MD, 2010.
(45) Clarke, G. M.; Cooke, D. *A Basic Course in Statistics*; 4th ed.; Arnold: New York, 1998.
(46) Choi, S. C. *Introductory Applied Statistics in Science*; Prentic-Hall, Inc.: Englewood Cliffs, NJ, 1978.
(47) Halász, G.; Gyüre, B.; Jánosi, I. M.; Szabó, K. G.; Tél, T. *Am. J. Phys.* **2007**, *75*, 1092.
(48) He, S.; Yao, J.; Jiang, P.; Shi, D.; Zhang, H.; Xie, S.; Pang, S.; Gao, H. *Langmuir* **2001**, *17*, 1571−1575.
(49) Linnert, T.; Mulvaney, P.; Henglein, A.; Weller, H. *J. Am. Chem. Soc.* **1990**, *112*, 4657−4664.
(50) Mostafavi, M.; Keghouche, N.; Delcourt, M.-O.; Belloni, J. *Chem. Phys. Lett.* **1990**, *167*, 193−197.
(51) Zhang, Z.; Patel, R. C.; Kothari, R.; Johnson, C. P.; Friberg, S. E.; Aikens, P. A. *J. Phys. Chem. B* **2000**, *104*, 1176−1182.
(52) Khan, S. A.; Senapati, D.; Senapati, T.; Bonifassi, P.; Fan, Z.; Singh, A. K.; Neeley, A.; Hill, G.; Ray, P. C. *Chem. Phys. Lett.* **2011**, *512*, 92−95.
(53) Prasad, B. L. V.; Stoeva, S. I.; Sorensen, C. M.; Klabunde, K. J. *Langmuir* **2002**, *18*, 7515−7520.
(54) Smetana, A. B.; Klabunde, K. J.; Sorensen, C. M. *J. Colloid Interface Sci.* **2005**, *284*, 521−526.
(55) Zhuang, J.; Wu, H.; Yang, Y.; Cao, Y. C. *Angew. Chem., Int. Ed.* **2008**, *47*, 2208−2212.
(56) García-Barrasa, J.; López-de-Luzuriaga, J. M.; Monge, M.; Soulantica, K.; Viau, G. *J. Nanopart. Res.* **2011**, *13*, 791−801.
(57) Lin, X. Z.; Terepka, A. D.; Yang, H. *Nano Lett.* **2004**, *4*, 2227−2232.
(58) Wagner, J.; Kirner, T.; Mayer, G.; Albert, J.; Köhler, J. M. *Chem. Eng. J.* **2004**, *101*, 251−260.
(59) He, S.; Kohira, T.; Uehara, M.; Kitamura, T.; Nakamura, H.; Miyazaki, M.; Maeda, H. *Chem. Lett.* **2005**, *34*, 748−749.
(60) Wagner, J.; Köhler, J. M. *Nano Lett.* **2005**, *5*, 685−691.
(61) Wang, J.; Song, G.; Peng, Y.; Zhu, Y. *Tetrahedron Lett.* **2008**, *49*, 6518−6520.